Available online at www.sciencedirect.com

ScienceDirect

Computational Geometry 40 (2008) 115–137

Computational Geometry
Theory and Applications

www.elsevier.com/locate/comgeo

Recursive geometry of the flow complex and topology of the flow complex filtration ☆

Kevin Buchin [a], Tamal K. Dey [b], Joachim Giesen [c,*], Matthias John [d]

[a] *Institute of Computer Science, Freie Universität Berlin, Takustraße 9, D-14195 Berlin, Germany*
[b] *Department of Computer Science and Engineering, The Ohio State University, 2015 Neil Avenue, Columbus, OH 43210, USA*
[c] *Max-Planck-Institut für Informatik, Department 1: Algorithms and Complexity, Stuhlsatzenhausweg 85, 66123 Saarbrücken, Germany*
[d] *Institut für Theoretische Informatik, ETH Zurich, Universitätstraße 6, 8092 Zürich, Switzerland*

Received 3 September 2006; received in revised form 19 February 2007; accepted 22 May 2007

Available online 21 June 2007

Communicated by O. Cheong

Abstract

The flow complex is a geometric structure, similar to the Delaunay tessellation, to organize a set of (weighted) points in $\mathbb{R}^k$. Flow shapes are topological spaces corresponding to substructures of the flow complex. The flow complex and flow shapes have found applications in surface reconstruction, shape matching, and molecular modeling. In this article we give an algorithm for computing the flow complex of weighted points in any dimension. The algorithm reflects the recursive structure of the flow complex. On the basis of the algorithm we establish a topological similarity between flow shapes and the nerve of a corresponding ball set, namely homotopy equivalence.

Keywords: Flow complex; Čech complex; Alpha shapes; Delaunay triangulation; Filtration; Homotopy equivalence

1. Introduction

1.1. Background

The flow complex of a set of points has been successfully applied to surface reconstruction from a point cloud [13], to shape segmentation and matching [5], and to modeling properties of macromolecules in bio-geometry [12]. It is a cell decomposition based on the flow in the direction of the steepest ascent of the power distance function to a given set of weighted points. It is closely related to the Voronoi diagram and the Delaunay tessellation, in particular in the case of weighted points it is related to the power diagram and the regular triangulation (see e.g. [8,21]). The flow

☆ Part of this research was supported by the Deutsche Forschungsgemeinschaft within the European graduate program 'Combinatorics, Geometry, and Computation' (No. GRK 588/2). Also partially supported by the IST Programme of the EU as a Shared-cost RTD(FET Open) Project under Contract No IST-006413 (ACS—Algorithms for Complex Shapes). Also supported by NSF CARGO grant DMS-0310642.
* Corresponding author.
E-mail address: giesen@inf.ethz.ch (J. Giesen).

0925-7721/$ – see front matter
doi:10.1016/j.comgeo.2007.05.005

complex was introduced by Giesen and John [13]. Discrete flow was first used in 1995 for surface reconstruction by Edelsbrunner [9] (see also [10]) who defined a flow relation on the simplices of the Delaunay tessellation.

For computing the flow complex so far only algorithms specializing on the two and three dimensional complex are known. For instance in the case of unweighted, two-dimensional points the complex corresponds to the Gabriel graph which can easily be computed using the Delaunay tessellation. Here we want to give insight into the general structure of the complex independent of the dimension. The analysis of its geometric structure leads to an algorithm for computing the flow complex of (weighted) points in any dimension, which reveals a recursive structure of the flow complex.

The algorithm is used to analyze topological properties of flow shapes. Flow shapes are obtained by restricting the influence of the points to a maximum distance α, i.e., to a ball of radius $\sqrt{\alpha}$ since we are considering the power distance. Varying the distance a yields a filtration of the flow complex, i.e., a family of nested sub-complexes. A flow shape is the topological space underlying a sub-complex. Note that we only refer to the final complex in the filtration as flow complex.

Flow shapes are shape constructors, i.e., they transform finite point sets into continuous shapes. The choice of the influence distance α for the points allows multi-scale modeling which turns out to be useful in detecting features at different scales. Due to their practical importance in geometric modeling various shape constructors have been proposed recently. Understanding the relationship among them leads to new insights potentially helpful in applications. An overview of various shape constructors and their relation is given by Carlsson and de Silva [3]. A comprehensive overview of computational topology is given by Zomorodian [26].

We place flow shapes in relation to these shape constructors by showing that the flow shape for a distance α is homotopy equivalent to the union of balls of radius $\sqrt{\alpha}$. For this we prove that a flow shape can be obtained from the corresponding union of balls by a deformation retraction. A natural representation of the topology of the union of balls is Čech complex of the balls. The Čech complex is the nerve of the ball set, i.e., it is the (abstract) simplicial complex with a vertex for every ball and a simplex for every subset of balls with non-empty intersection. By the *nerve lemma* [18], the Čech Complex and the union of balls are homotopy equivalent.

The Čech complex might have a large number of simplices and in particular higher-dimensional simplices. The α-shape complex [11] is a simplicial complex (with a scale parameter α) that has the same homotopy type as the Čech complex [7] but is embedded in $\mathbb{R}^k$ and has much fewer simplices. When varying α, the Čech complex and therefore also the α-shape complex and the flow shapes change their homotopy type only at discrete critical levels. An illustration of these complexes for different values of α is given in Fig. 10 in Section 6.1. In contrast to the other two complexes, the geometry of the flow shapes changes only at these critical levels. Thus, the flow complex filtration precisely captures the topological changes of the family of Čech complexes parametrized by α. Furthermore the definition of flow shapes has a strong Morse theoretic flavor which might allow the use of Morse theoretic concepts [14,15,20].

Preliminary versions of this work appeared in [2] and [6].

1.2. Introductory example

Algorithm. In Section 5 we present an algorithm for constructing the flow complex of a set of points. The algorithm computes the inflow into any critical point of the distance to a point set. Flow here is with meant with respect to the direction of steepest ascent of this distance function and a critical point is a point with no unique direction of steepest ascent (later we will make these concepts more precise). The basic concept of the algorithm is to first compute the points that flow directly (on a straight line segment) into the critical point, then the direct flow into these points, and so on. We illustrate this by the simple example of Fig. 1 with three input points (see Section 5.1 for a more complex example). By definition the flow at a point in the plane is in the direction in which the Euclidean distance to the closest input point (or points) increases most. Fig. 1(a) shows the three input points (black dots) and a critical point ($\oplus$) of the flow. This critical point is a local maximum of the distance function. The flow into this critical point can be computed as follows: We start with the point itself. Direct flow into this point lies either on a line segments between one of the input points and the critical point or on one of the bisectors of two input points. This gives as direct flow the six (open) line segments shown in Fig. 1(b). Next, we consider the direct flow into these line segments. There is only flow into the line segments on bisectors. Into each of these line segments there is flow from two (open) triangles shown in Fig. 1(c). There is no flow into these triangles. Thus the total flow into the critical point is the open triangle spanned by

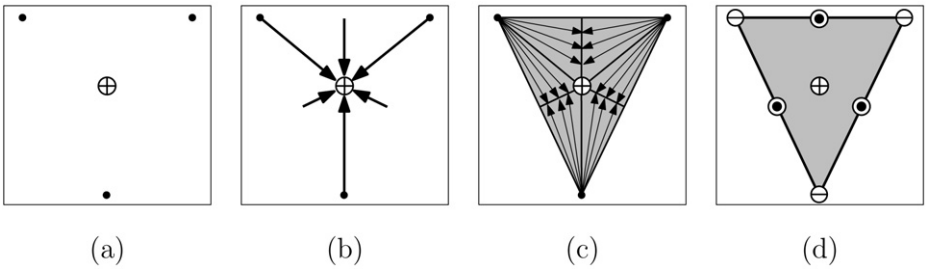

Fig. 1. Illustration of the recursive structure.

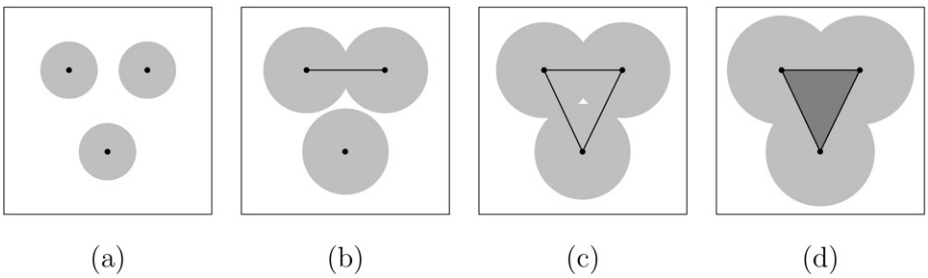

Fig. 2. Filtration of a flow complex.

the input points. The flow in the example has six further critical points: the input points themselves (which are minima of the distance function and have themselves as inflow region) and the midpoints of the line segments between the input points (which are saddle points of the distance function and have the open line segments between the points as inflow region). The flow complex is shown in Fig. 1(d).

Homotopy equivalence. In Section 6 we construct for all values of α a deformation retraction from the union of balls to the flow shape, i.e., the flow shape can be obtained by continuously shrinking the union of balls. For an illustration consider Fig. 2 with the same input points as above. It shows the filtration of the flow complex in comparison to the union of balls (see Fig. 10 for a comparison of flow shapes to other shape constructors and Fig. 13 for an example with points sampled from a surface). For $\alpha = 0$ the union of balls consists of the three input points. The flow shape is the underlying space of the cells corresponding to critical points covered by the union of balls. Thus, for $\alpha = 0$ the flow shape also consists of the three input points and is therefore equal to the union of balls. When α is increased, the balls grow but can be continuously shrunken back to the point set as long as none of the balls overlap (Fig. 2(a)). In Fig. 2(b) a pair of balls overlap. The area of overlap contains a critical point of the flow and the corresponding cell has been added to the flow shape. The flow shape now consists of a line segment and a point. As before the flow shape can be obtained by continuously shrinking (but no longer only radially) the union of balls, thus the flow shape and union of balls are again homotopy equivalent. When increasing α further, first the two other pairs of balls intersect and the corresponding line segments are added to the flow shape (Fig. 2(c)). Eventually all three balls overlap and the cell constructed in the previous example is added to the shape (Fig. 2(d)).

To construct the deformation retraction, the algorithm for the flow complex can be used in the following way: Assume we have constructed the deformation retraction for Fig. 2(c) and now want to construct it for Fig. 2(d). In Fig. 2(d) reducing α slightly (e.g. to the value of Fig. 2(c)) will leave a small part of the flow shape uncovered. After removing this small part we can follow the steps of the algorithm to continuously shrink the corresponding cell of the flow complex to its boundary, and thus shrink the flow shape to the flow shape of Fig. 2(c). Then, by again adding all parts removed we extend the deformation retraction of Figs. 2(c) to 2(d).

2. Preliminaries

In this article we discuss geometric data structures on weighted points in $\mathbb{R}^k$ and their topological relation. We first give a brief introduction to Voronoi diagrams and Delaunay tessellations together with some basic geometric

concepts. Then we consider underlying concepts from topology and introduce the union of balls, the Čech complex and the α-shape complex.

For a more detailed introduction to these concepts we refer to Matoušek [19] for fundamental geometric notions, Ziegler [25] for polytopes and polyhedra, to Okabe et al. [21] and Edelsbrunner [8] for Voronoi diagrams and Delaunay tessellations, to Bredon [1] and Hatcher [17] for homotopy, and to Carlsson and de Silva [3] for the union of balls and the Čech complex.

Notations are summarized in Appendix A at the end of the article.

2.1. Voronoi diagram and Delaunay tessellation

The Voronoi diagram and its dual Delaunay tessellation are a way to structure a set P of (possibly weighted) points in $\mathbb{R}^k$. The Voronoi diagram partitions the space into regions with common closest neighbor in the point set P, while the Delaunay tessellation links points in P if their Voronoi regions have a common face. The Voronoi diagram is a polyhedral complex. The Delaunay tessellation is a polytopal complex, and furthermore simplicial if the points (and for weighted points the corresponding balls) are in general position.

The Voronoi diagram of weighted points is also called *power diagram* and the Delaunay tessellation of weighted points *regular triangulation*. In the following the term *point* always refers to a weighted point and the terms *Delaunay tessellation* and *Voronoi diagram* always include also the weighted versions.

Weighted points and power distance. A *weighted point* is a point $p \in \mathbb{R}^k$ together with a *weight* w_p, also called *power*.

The *power distance* of a point $x \in \mathbb{R}^k$ from a weighted point p is defined as

$$\pi_p(x) = \|x - p\|^2 - w_p.$$

If w_p and $\pi_p(x)$ are positive and the dimension k is at least two, the power distance from x to p has the following geometric interpretation: consider the sphere with radius $\sqrt{w_p}$ around p. Let t be a point on the sphere and on a tangent line through x. Then by the Pythagorean theorem $\pi_p(x) = \|x - t\|^2$.

Relative interior and boundary. We always refer to the interior and to the boundary of convex sets with respect to their dimension, i.e., to their relative interior and boundary.

Let $\mathit{aff}(C)$ denote the affine hull of C. The *relative interior* C° and the *relative boundary* ∂C of C are the interior and the boundary of C in $\mathit{aff}(C)$. For instance the relative interior of a Delaunay edge contains all points in this edge besides the endpoints, i.e., the interior relative to the line through the edge.

The closure of C will be denoted by $\overline{C}$.

Complexes. A *polyhedral complex* [25] $\mathcal{C}$ is a finite collection of polyhedra in $\mathbb{R}^k$ such that

- the empty polyhedron is in $\mathcal{C}$,
- if $C \in \mathcal{C}$ then all the faces of C are also in $\mathcal{C}$,
- the intersection $C_1 \cap C_2$ of two polyhedra $C_1, C_2 \in \mathcal{C}$ is a face both of C_1 and of C_2.

For polytopes C_1, C_2 we will denote by $C_1 \leqslant C_2$ (and by $C_2 \geqslant C_1$) that C_1 is a face of C_2 (and C_2 a co-face of C_1) and by $C_1 < C_2$ (and by $C_2 > C_1$) that C_1 is a proper face of C_2 (and C_2 a proper co-face of C_1).

If the cells of a polyhedral complex $\mathcal{C}$ are all bounded then $\mathcal{C}$ is called *polytopal complex*. If the cells are all simplices then $\mathcal{C}$ is called (*geometric*) *simplicial complex*. The combinatorial structure of a simplicial complex on n vertices is captured by an *abstract simplicial complex*, i.e., a family of subsets of $\{1, \ldots, n\}$ that is closed under taking subsets.

Voronoi diagram. Let P be a finite set of (weighted) points in $\mathbb{R}^k$. The *Voronoi cell* of the (weighted) point $p \in P$ is given as

$$V_p = \left\{x \in \mathbb{R}^k \mid \forall q \in P, \pi_p(x) \leqslant \pi_q(x)\right\}.$$

The sets V_p are (possibly empty) convex polyhedra since the set of points that have the same power distance from two points in P forms a hyperplane.

The faces of Voronoi cells (including the empty face and the cell itself) are called *Voronoi faces*. The *Voronoi diagram* $V(P)$ of P is the collection of all *Voronoi faces*.

For computing the flow complex the relative interiors and boundaries of (the underlying space of) Voronoi faces will play a central role. The relative boundary of a Voronoi face is (the underlying space of) the union of its proper faces.

Delaunay tessellation. The *Delaunay tessellation* of a point set P in $\mathbb{R}^k$ is the dual of the Voronoi diagram of P. The Delaunay tessellation is a polytopal complex with the convex hull of P as underlying space. Its vertex set is P. A k-dimensional *Delaunay cell* is defined by $k+1$ or more points in P if the intersection of their corresponding Voronoi cells is a vertex of the Voronoi diagram.

For two points p and q the set of all points with the same power distance to p and q is a hyperplane orthogonal to the line through p and q. This yields the following relation between a Voronoi face and its dual Delaunay face which we will use to derive properties of the flow complex.

Remark 1. The affine hulls of a Voronoi face and its dual Delaunay face are orthogonal and intersect in exactly one point.

2.2. Homotopy

Homotopy equivalence and deformation retract. A *homotopy* is a continuous map $F : X \times [0,1] \to Y$. Two continuous maps $f_1, f_2 : X \to Y$ are *homotopic* (denoted by $f_1 \simeq f_2$), if there is a homotopy connecting them, i.e., $f_1(x) = F(x,0)$ and $f_2(x) = F(x,1)$.

A continuous map $f : X \to Y$ is called *homotopy equivalence* if there is a continuous map $g : Y \to X$ with $fg \simeq id_Y$ and $gf \simeq id_X$, where id_Y and id_X denote the identity map on Y and on X, respectively. In this case the spaces X and Y are said to be *homotopy equivalent* or to have the same *homotopy type*, denoted by $X \simeq Y$.

A homotopy $F : X \times [0,1] \to X$ is called *deformation retraction* of X to a subspace A if $F(x,0) = x$ for all $x \in X$, $F(X,1) = A$, and $F(a,t) = a$ for all $a \in A$ and $t \in [0,1]$. In this case $A \simeq X$ and A is called a *deformation retract* of X.

Mapping cylinder neighborhood. The following topological concepts are used in the proof of Theorem 16. For a more detailed and illustrated introduction to these concepts we refer to the text book by Hatcher [17].

The *mapping cylinder* M_f of a continuous map $f : X \to Y$ is the quotient space of the disjoint union of $X \times [0,1]$ and Y formed by identifying $(x,0)$ of $X \times \{0\}$ with the point $f(x)$ in Y. A subspace A of X has a *mapping cylinder neighborhood* N in X if the neighborhood N contains a subspace B such that $N - B$ is an open neighborhood of A and there is a continuous map $f : B \to A$ and a homeomorphism $h : M_f \to N$ which is constant on $A \cup B$.

We will use the following property of such a pair (X, A) (see [17, Example 0.15 and Corollary 0.20]):

Remark 2. If A has a mapping cylinder neighborhood in X and the inclusion $A \hookrightarrow X$ is a homotopy equivalence, then A is a deformation retract of X.

2.3. Union of balls and Čech complex

Union of balls. For the power distance of a point p with positive weight w_p, $\sqrt{w}$ was interpreted as radius of a ball around p. Similarly, for a parameter α we will consider the *family of balls* $B_\alpha(P)$ with radii $\sqrt{\alpha + w_p}$ for all $p \in P$ with $\alpha + w_p \geqslant 0$. Thus with P_α defined as

$$P_\alpha := \{p \in P \mid \alpha + w_p \geqslant 0\}$$

the *union of balls* is the underlying space of $B_\alpha(P)$, i.e.,

$$\big|B_\alpha(P)\big| := \bigcup_{b \in B_\alpha(P)} b = \big\{x \in \mathbb{R}^k \mid \exists p \in P_\alpha \text{ such that } \pi_p(x) \leqslant \alpha\big\}.$$

Čech complex. The Čech complex $\check{C}_a(P)$ is the *nerve* [24] of the family of balls $B_\alpha(P)$, i.e., the simplicial complex with $B_\alpha(P)$ as vertex set and a simplex for every subset of balls with non-empty intersection. By the *nerve lemma* [18], the Čech complex and the union of balls are homotopy equivalent.

The subcomplex obtained by restricting to the simplices for which the Voronoi cells corresponding to the balls share a (non-empty) face is the *α-shape complex*. It is a subcomplex of the Delaunay tessellation and is homotopy equivalent to the Čech complex [7].

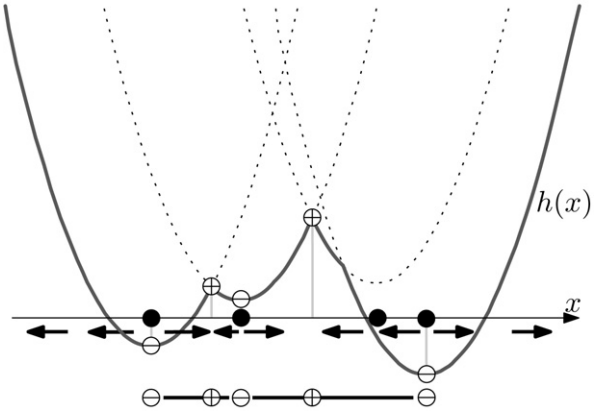

Fig. 3. One-dimensional example of flow induced by a set of weighted points.

3. Flow and the flow complex

3.1. The distance function and its critical points

Distance function. The flow that we are going to study is the flow in direction of the steepest ascent of the *distance function*

$$h(x) = \min\{\pi_p(x) \mid p \in P\}$$

induced by the points in P.

Fig. 3 shows a one-dimensional example with weighted points. The points in P are shown as black dots. The weight w_p of a point p is the signed distance from the point to the apex of the parabola below (positive weight) or above (negative weight) it. The graph of the distance function h is the lower envelope of the parabolas.

Critical and regular points. For a smooth function the direction of steepest ascent corresponds to the direction of the gradient. Here, h is not smooth on the boundary of Voronoi cells but the notion of *generalized gradients* is applicable. Generalized gradients have been defined in the context of critical point theory for distance functions on Riemannian manifolds [4,15,22] pioneered by Grove and Shiohama [16].

In the case of the Euclidean space $\mathbb{R}^k$ as Riemannian manifold and h as distance function, generalized gradients can be described as follows: Let $N(x) \subset P$ be the set of nearest neighbors of x in P, i.e., the set of all $p \in P$ with $\pi_p(x) = h(x)$. For a point $x \in \mathbb{R}^k$ the set of *generalized gradients* at x is the set of unit vectors $v \in \mathbb{R}^k$ pointing away from all points in $N(x)$, i.e., for which

$$\langle v, x - p\rangle > 0 \quad \text{for all } p \in N(x).$$

For instance, if $N(x)$ only contains one point then h is smooth in x and the generalized gradient is the open hemisphere with the unit vector in direction of the gradient as center.

A point is called *critical* if the set of generalized gradients is empty, otherwise it is called *regular*. Thus, a point $x \in \mathbb{R}^k$ is critical if and only if $x \in \mathit{conv}(N(x))$. If $x \in \partial\mathit{conv}(N(x))$, then it is a *degenerate* critical point. In the following we assume that all critical points are non-degenerate. The definition directly yields a description of the critical points in terms of the Voronoi diagram and the Delaunay tessellation. The convex hull $\mathit{conv}(N(x))$ is the Delaunay face dual to the Voronoi face corresponding to $N(x)$ in which x lies.

Remark 3. The critical points of h are exactly the intersections of Voronoi faces and their dual Delaunay faces.

In the one-dimensional example of Fig. 3 the critical points are the local maxima ($\oplus$) and minima ($\ominus$) of the distance function h. In higher dimensions saddle points are further critical points. In the case of weighted points as in the example, points in P are not necessarily minima, thus not necessarily critical points. The arrows below the x-axis indicate the direction of the generalized gradient which is unique in the one-dimensional case.

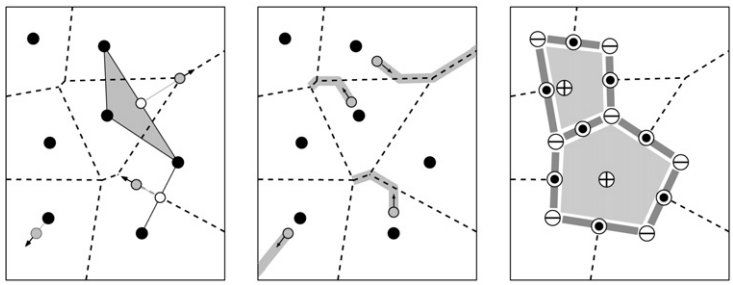

Fig. 4. Two-dimensional example of flow induced by a set of unweighted points.

In the following we define a vector field in accordance with this theory. We will prove later that the vector at a regular point corresponds to the direction of steepest ascent of the distance function.

3.2. A vector field of generalized gradients

Vector field and drivers. For $x \in \mathbb{R}^k$ the point

$$d(x) = \operatorname*{argmin}_{y \in conv(N(x))} \|x - y\|^2$$

is called the *driver* of x.

We define a vector field $v : \mathbb{R}^k \to \mathbb{R}^k$ by

$$v(x) := \begin{cases} \frac{x-d(x)}{\|x-d(x)\|} & \text{if } x \text{ is a regular point of } h, \\ 0 & \text{otherwise.} \end{cases}$$

The drivers and vectors are illustrated in Fig. 4(a) for a set P of unweighted points in $\mathbb{R}^2$. The points in P are shown as black dots and the 1-skeleton of their Voronoi diagram as dashed lines. For the three gray points the corresponding drivers are shown and the corresponding vectors are indicated as arrow. For the gray point in the interior of a Voronoi cell of a point p the driver is the point p. For the gray point on a Voronoi segment the driver shown as white point is the intersection of the Voronoi segment and the dual Delaunay segment. For the gray point at a Voronoi vertex the driver shown as white point is the closest point on the dual Delaunay triangle.

Flow. The *flow* $\phi : [0, \infty) \times \mathbb{R}^k \to \mathbb{R}^k$ is defined by the equations

$$\phi(0, x) = x,$$
$$\lim_{t \downarrow t_0} \frac{\phi(t, x) - \phi(t_0, x)}{t - t_0} = v\big(\phi(t_0, x)\big).$$

If the first parameter is interpreted as time then $\phi(t, x_0)$ can be interpreted as the point reached at time t by starting at time 0 at x_0 and following the direction given by v. For $x_0 \in \mathbb{R}^k$

$$\phi_{x_0}(t) := \phi(t, x_0)$$

is called the *orbit* of x_0. Fig. 4(b) shows the orbits for some points for the two-dimensional example used before.

If $\phi(t, x_0) = x_0$ for all $t \geqslant 0$ then x_0 is a *fixed point* of the flow. The fixed points of the flow are exactly the critical points of the distance function h.

3.3. The flow complex

Stable manifolds. Points in $\mathbb{R}^k$ flow either into a critical point or to infinity as Fig. 4(b) indicates. We are interested in a decomposition of $\mathbb{R}^k$ into regions $S(c)$ such that all points in a region flow into the same critical point c, i.e., the *stable manifold* of c

$$S(c) = \big\{x \in \mathbb{R}^k \mid (\exists t \geqslant 0)\phi(t, y) = c\big\}.$$

Note that the points that flow to infinity do not lie in the stable manifold of a critical point. To obtain a decomposition of R^k we could add a designated critical point at infinity.

Flow complex. The *flow complex* is the collection of closures of the stable manifolds of all critical points (not including a critical point at infinity).

For the one-dimensional example of Fig. 3 the stable manifolds are line segments and points. They are shown below the graph. The stable manifold of a minimum is the minimum itself. The stable manifold of a maximum is a full-dimensional open set, i.e., a segment in the one-dimensional example. The flow complex in this example contains the three minima and the two (closed) segments between them.

For the two-dimensional example the stable manifolds are shown in Fig. 4(c). The distance function h has two maxima, and their stable manifolds are the interiors of the two polygons depicted. The open segments on their boundary are the stable manifolds of the saddle points of h and the vertices are the stable manifolds of the minima, i.e., the points in P. The flow complex is the closure of these stable manifolds, i.e., the two polygons and the segments and vertices on their boundaries.

4. Properties of the flow

Most of the properties proved in this section are needed to prove the correctness of the algorithm in the next section. Most important for the algorithm is the fact that all points in the interior of a Voronoi face have the same driver (Lemma 4). To bound the depth of recursion in the algorithm it is essential that any orbit passes through a Voronoi face at most once (Theorem 9). (The reader who wishes to see the algorithm first can skip the derivation of these properties and proceed to Section 5 without losing the main stream.)

Besides the properties needed in the algorithm we prove a fundamental fact concerning the vector field considered: The vector $v(x)$ at a regular point $x \in \mathbb{R}^k$ corresponds to the direction of steepest ascent of $h(x)$ (Theorem 10).

The following lemma yields a description of drivers in terms of Voronoi diagrams. In particular it yields that the number of Voronoi faces is an upper bound on the number of drivers. In the algorithm for computing the flow complex we use it to compute drivers and to treat the flow within a Voronoi face uniformly.

Lemma 4. *Let V be an arbitrary Voronoi face and D its dual Delaunay face. Then all points x in the interior of V have the same driver d which is the point in D closest to $\mathit{aff}(D) \cap \mathit{aff}(V)$.*

Proof. The proof is illustrated in Fig. 5. Note that for this example the weight of the left vertex of D must be small compared to the weight of the right vertex.

Let D be the Delaunay face dual to V and let z be the intersection point of the affine hulls $\mathit{aff}(V)$ and $\mathit{aff}(D)$ (see Remark 1). Let $d \in D$ be the point closest to z. Note that it is possible that $d = z$.

Let y be any point in D. Since $y - z$ is orthogonal to $x - z$ we have by Pythagorean theorem (denoted in the following by P.t.)

$$\|x - y\|^2 \overset{\text{P.t.}}{=} \|x - z\|^2 + \|y - z\|^2 \geqslant \|x - z\|^2 + \|d - z\|^2 = \|d - x\|^2.$$

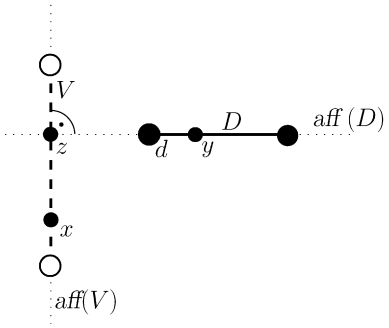

Fig. 5. Illustration of the proof of Lemma 4.

Thus d is the closest point in $D = conv(N(x))$ to x and therefore its driver. The argument holds for any point having V as lowest dimensional Voronoi face containing it, i.e., for all points in V°. □

For a point x in the Voronoi cell of p we have $h(x) = \pi_p(x)$, thus h is determined by the power distance to its driver. To generalize this we assign a power to every driver. We show in the following lemma that with these powers $h(x)$ is determined by $\pi_{d(x)}$ for all x. The power of a driver will be used as a tool to prove the acyclicity of the flow.

For a driver d let D be the lowest dimensional Delaunay face that contains d, and let p be a vertex of D. We define

$$w_d = -\pi_p(d).$$

Observe that the value w_d is independent of the choice of p, as follows from the following lemma. The intuition behind this definition is that the graphs of the distance functions π_p of the vertices p of D intersect in a lower-dimensional paraboloid with apex d and weight w_d.

Lemma 5. *For a Voronoi face V and the driver d of V°*

$$h(x) = \pi_d(x) \quad \textit{for all } x \in V.$$

Proof. Let $p' \in P$ be a vertex of the lowest dimensional Delaunay face D' containing d. In particular, p' is a point defining V, thus

$$h(x) = \pi_{p'}(x)$$

for any point $x \in V$. Since D' is a convex polytope and d is the closest point on D' to x, $x - d$ and $p' - d$ are orthogonal.

Therefore,

$$\begin{aligned} h(x) = \pi &= \|p' - x\|^2 - w_{p'} \\ &\overset{\text{P.t.}}{=} \|d - x\|^2 + \|p' - d\|^2 - w_{p'} = \|d - x\|^2 + \pi_{p'}(d) = \|d - x\|^2 - w_d = \pi_d(x). \end{aligned}$$ □

Like π_p for $p \in P$ the power distance π_d of a driver has the property that it is never below h.

Lemma 6. *For a driver d*

$$h(x) \leqslant \pi_d(x) \quad \textit{for all } x \in \mathbb{R}^k.$$

If D is the lowest dimensional Delaunay face containing d and V its dual Voronoi face then

$$h(x) < \pi_d(x) \quad \textit{for all } x \notin \textit{aff}(V).$$

Proof. Let p be a vertex of D. By definition of w_d we have

$$\pi_d(x) = \|x - d\|^2 + \|d - p\|^2 - w_p.$$

Thus, $\pi_d(x) \geqslant \pi_p(x)$ if and only if the angle $\measuredangle(p, d, x) \leqslant \pi/2$ by the law of cosines. Since $d \in D$ and D is convex this holds for at least one of the vertices $p \in D$. If $x \notin \textit{aff}(V)$ then there is a vertex $p \in D$ with $\measuredangle(p, d, x) < \pi/2$. □

The following lemma provides a condition under which a Voronoi face V shares its driver with a co-face V' of V.

Lemma 7. *Let V be a Voronoi face with co-face V'. Let d and d' be the drivers of V° and V'°, respectively. If no line segment connecting a point of V with d' intersects V'° then $d = d'$. Otherwise, $d \neq d'$ and $w_d < w_{d'}$.*

Proof. Let D and D' be the Delaunay faces dual to V and V', respectively. Since $V < V'$, we have $D > D'$. Let y be any point in the interior of V. Let z be the intersection point of the affine hull of D and V (see Remark 1). As $y \in V$ and $d, d' \in D$, $d - z$ and $d' - z$ are orthogonal to $y - z$.

First we prove

$$w_{d'} - w_d = \|z - d'\|^2 - \|z - d\|^2$$

which is equivalent to $\pi_{d'}(z) = \pi_d(z)$.

We have

$$\pi_d(z) = \|d-z\|^2 - w_d \overset{\text{P.t.}}{=} \|d-y\|^2 - \|y-z\|^2 - w_d = \pi_d(y) - \|y-z\|^2 = h(y) - \|y-z\|^2$$

and by the same argument $\pi_{d'}(z) = h(y) - \|y-z\|^2$. Thus, $\pi_{d'}(z) = \pi_d(z)$.

Now we show that if the line segment $L_{y,d'}$ from y to d' intersects the interior of V', we have $\|z-d'\| > \|z-d\|$ which implies $w_{d'} > w_d$ and that we get $d = d'$ otherwise. This part of the proof is illustrated in Fig. 6. Note that in the example of Fig. 6(b) the weight of w_q must be large relative to w_p.

Let H_1 be the affine hull of D. Let H_2 be the hyperplane through d' orthogonal to $L_{y,d'}$. H_1 is subdivided by H_2 in two half-subspaces. D' is in the closed half-subspace not containing y since D' is convex and d' is the closest point of D' to y.

Let q be any Delaunay vertex of D which is not a vertex of D'. The point q lies in the same half-subspace of H_1 as the convex hull of $D' \cup \{q\} \subset D$ and the point d' lies in D'. So if q lies in the same half-subspace as z as in the case of Fig. 6(a) there is a point of D closer to z than d' and therefore $\|z-d'\| > \|z-d\|$. If any such q lies in a different half-subspace than z as in the case of Fig. 6(b) then d' is the closest point of D to z and thus

$$\|z-d'\| = \|z-d\|.$$

If $L_{y,d'}$ intersects V' then q lies in the same half-subspace as z. Otherwise they lie in different half-subspaces. This proves the lemma. □

A consequence of this lemma is the following.

Lemma 8. *For all $y \in \mathbb{R}^k$ there is an $\varepsilon_0 > 0$ such that*

$$d\big(y + \varepsilon v(y)\big) = d(y) \quad \textit{for all } 0 < \varepsilon < \varepsilon_0.$$

Proof. Let V be the Voronoi face with $y \in V^\circ$. For a sufficiently small $\varepsilon > 0$

$$y' := y + \varepsilon v(y) \in V'^\circ$$

with V' a Voronoi face fulfilling $V \leqslant V'$.

For $V = V'$ we have $d(y) = d(y')$. Assume $V < V'$ and $d(y) \neq d(y')$. Thus, by Lemma 7 $L_{d(y'),y}$ intersects the interior of V'. For an illustration refer again to Fig. 6 but now with the driver d placed beyond z. Let H be the hyperplane orthogonal to $L_{d(y),d(y')}$ containing y. Since the vector from $d(y)$ to y points into V' and the vector from $d(y')$ to y out of V', $d(y)$ and $d(y')$ lie on different sides of H. But then the intersection of H with $L_{d(y),d(y')}$ is closer to y than $d(y)$ and lies inside D, contradicting that $d(y)$ is the driver of y. □

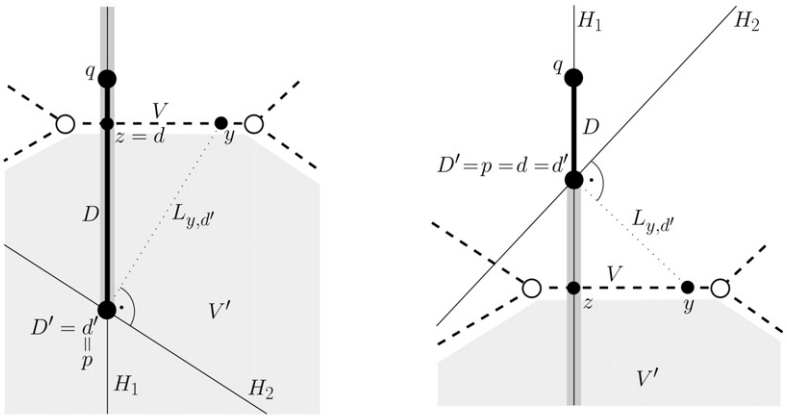

(a) $L_{y,d'}$ intersects V' and $d \neq d'$. (b) $L_{y,d'}$ does not intersect V' and $d = d'$.

Fig. 6. The two possible cases in Lemma 7.

Theorem 9 *(Orbits). The orbit of a point is a polygonal chain (possibly ending with a ray to infinity). The orbit passes through each Voronoi face at most once. The weights of the drivers increase along an orbit.*

Proof. For Voronoi faces V, V' with $V < V'$ Lemma 7 yields that the power of the driver along the orbit stays the same if the orbit goes from V° to V'° and strictly increases if it goes from V'° to V°. In the second case the driver changes and a line segment of the polygonal chain ends. Thus, we have an increasing sequence of drivers along an orbit and the orbit cannot enter a Voronoi face multiple times. □

Theorem 10 *(Steepest ascent). For all regular points $x \in \mathbb{R}^k$, the vector $v(x)$ points in the direction of steepest ascent.*

Proof. At a point $x \in \mathbb{R}^k$ with driver d by Lemma 5, $h(x) = \pi_d(x)$. For a sufficiently small $\varepsilon_0 > 0$, we have by Lemma 8 that d is the driver of all points $x + \varepsilon v(x)$ for all $0 \leqslant \varepsilon < \varepsilon_0$ and therefore

$$h\big(x + \varepsilon v(x)\big) = \pi_d\big(x + \varepsilon v(x)\big).$$

For all unit vectors v' we have

$$h(x + \varepsilon v') \leqslant \pi_d(x + \varepsilon v') \leqslant \pi_d\big(x + \varepsilon v(x)\big) = h\big(x + \varepsilon v(x)\big),$$

where the first inequality follows from Lemma 6, the second inequality from the definition of π_d and v, and the last equality from the argument above. If $v' \neq v(x)$ the second inequality holds strictly, thus, $v(x)$ is the direction of steepest ascent at x. □

5. The flow complex and its recursive structure

Outline. The flow complex consists of the closures of the stable manifolds of the critical points of the distance function. Thus, in order to compute the flow complex we need to compute these closures.

We present an algorithm that computes the stable manifold for a given critical point. The algorithm makes use of the close relationship of the flow complex to the Delaunay tessellation and the Voronoi diagram of P. The critical points can be determined using their description as intersections of Voronoi faces and their dual Delaunay faces (Remark 3). The algorithm yields a description of the closure of a stable manifold as a polytopal complex.

5.1. Example

Before presenting the algorithm we illustrate the recursive nature of the flow by the example of Figs. 7 and 8. Fig. 7(a) shows a set of four weighted points together with its Voronoi diagram and Fig. 7(b) shows the stable manifold

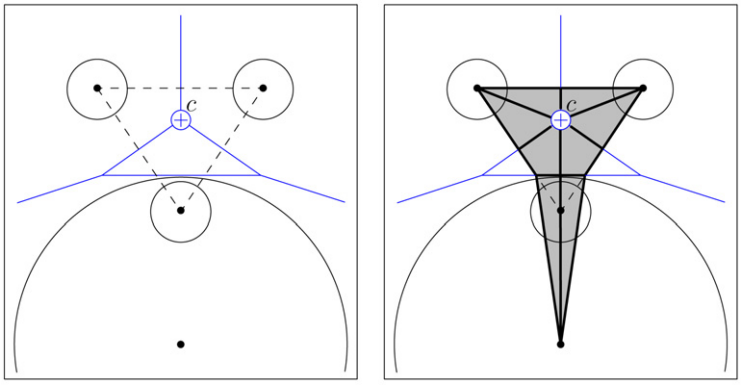

(a) weighted point set (b) stable manifold of c

Fig. 7. A decomposition of a stable manifold as computed by the algorithm.

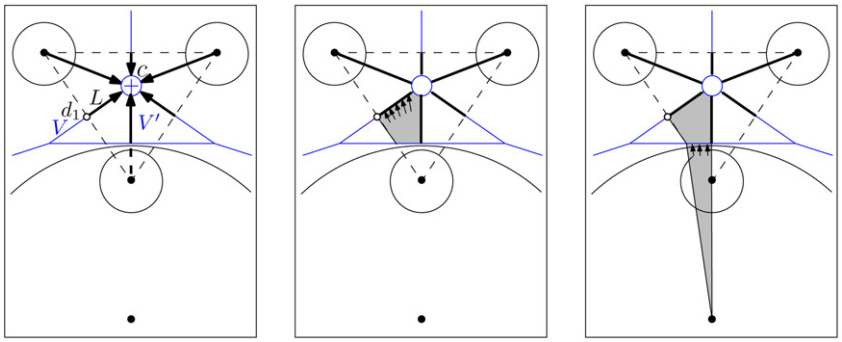

(a) inflow into c (b) inflow into L from V' (c) inflow into C_1

Fig. 8. Several steps in the computation of the stable manifold of c.

of the local maximum c. The points are depicted as black dots. Their weights are depicted by the circles, where the weight of a point corresponds to the squared radius of a circle. To demonstrate effects that do not appear in the unweighted two-dimensional case, one of the points has a very large weight. As a consequence one of the points does not lie in its Voronoi cell and the closure of the stable manifold has non-simplicial cells.

We want to compute the stable manifold of the local maximum c of h depicted as $\oplus$. Thus, we want to compute the *inflow* into c, i.e., all points eventually flowing into c. The orbits of points flowing into c are polygonal chains ending at c (Theorem 9). Therefore, any point flowing into c either lies on a line segment flowing into c or flows into a line segment flowing into c. To such a line segment we have a corresponding driver, thus we have only a finite number of such line segments (Lemma 4). In terms of inflow we have that the inflow into c is the union of these line segments and their inflow. This already indicates the recursive nature of the flow.

Fig. 8(a) shows the line segments flowing into c. Consider the line segment L and the driver d_1 of the Voronoi segment V in the figure. Thus all points between d_1 and c are driven into c by d_1. In general any line segment flowing directly into c must flow through a co-face of the Voronoi face of c and is driven by the driver of the interior of the co-face.

Next consider the inflow into L. Since L (without its endpoints) lies in the interior of the Voronoi segment V, inflow into L must again come from co-faces of V. In the example there is inflow coming from both neighboring Voronoi cells. Consider the inflow coming from V' as depicted in Fig. 8(b). The driver of V'° is d_2. All points of V' between L and d_2 are driven by d_2 into L. Since d_2 lies outside of V' the resulting set of points C_1 is $conv\{L, d_2\}^\circ \cap V'$.

Now V' is a Voronoi cell, so there is no inflow from co-faces of V'. But since d_2 was cut off from C_1 by the boundary of V', inflow coming from this boundary must be considered. The inflow into C_1 comes from C_2. The driver d_3 lies in its Voronoi cell and is therefore not cut off.

Computing all inflow into c in this way yields the stable manifold of c as depicted in Fig. 7(b).

5.2. Algorithm

Next we formulate the algorithm to compute the stable manifold of a critical point c, i.e., the inflow into c. The recursive nature of the flow as illustrated in the example above yields that the inflow into the relative interior C° of a convex set C is the set of all points flowing along a straight line into C° plus the inflow into these points. We therefore formulate the algorithm INFLOW with a parameter C. To compute the stable manifold of c we call the algorithm with $C = \{c\}$.

The Voronoi faces from which points might flow directly into C° can be easily determined if we know that C° lies in V° for a Voronoi face V. We therefore keep track of this face as a second parameter of the algorithm. To compute the stable manifold of c this parameter is set to the lowest dimensional Voronoi face V containing c. Relative interiors are used to get a unique decomposition of the Voronoi diagram and the stable manifolds. We can now formulate the algorithm.

INFLOW(CONVEX POLYTOPE C, VORONOI FACE V)
1 $\mathcal{I} := \{C\}$
2 **for each** Voronoi face V' with $V < V'$ **do**
3 $d :=$ driver of V'°
4 $C' := conv(C, d)$
5 **if** $C'^\circ \cap V \not\subseteq C$ **do**
6 $\mathcal{V} := \{V'' \leqslant V' \mid C'^\circ \cap (V'')^\circ \not\subseteq V\}$
7 **for each** $V'' \in \mathcal{V}$ **do**
8 $\mathcal{I} := \mathcal{I} \cup$ INFLOW$(C' \cap V'', V'')$
9 **end for**
10 **end if**
11 **end for**
12 **return** $\mathcal{I}$

We first describe how the algorithm works and then prove its correctness in Theorem 11. We do not claim the algorithm to be optimal and do not analyze the complexity of the algorithm beyond proving that it terminates. Nonetheless, its complexity would be of interest in particular as an upper bound for the complexity of the flow complex. The algorithm is polynomial in the number of *combinatorially different* orbits, where we call two orbits combinatorially different if they traverse a different sequence of Voronoi faces.

Since the inflow has to contain C we add C to it in line 1 of the algorithm. We have to take care of the inflow into the relative interior of C that comes through the boundary of V or through higher dimensional Voronoi faces that contain V in their boundary. Since the algorithm INFLOW only takes care of the higher dimensional Voronoi faces we need to guarantee that any flow coming through the boundary of V has been handled when INFLOW is called.

Note that in the special case of $C = \{c\}$ there cannot be any inflow from within the Voronoi face V (and thus from the boundary of V) since in this case c is the unique driver of the relative interior of V that pushes away all other points in this relative interior (Lemma 4).

In the loop in lines 2 to 11 we take care of the inflow via all Voronoi faces V' that contain V in their boundary. The relative interior of any Voronoi face V' has a unique driver d that we determine in line 3 (using (Lemma 4)). All points that flow via V' into the relative interior of C have to be contained in the intersection of V' with the relative interior of the pyramid C' whose apex is d and whose base is C. If V' does not contain its driver d, i.e., if d is not a critical point, then the whole pyramid cannot be contained in V' but is cut off at the boundary of V'. This can result in a non-simplicial cell as the example of C_1 in Fig. 8(b) shows.

In lines 5 to 10 we take care of the inflow coming from V' and its boundary. By definition V' is in $\mathcal{V}$ therefore the inflow into the cut-off pyramid coming from higher-dimensional Voronoi faces is computed by a recursive call of the algorithm in line 8. By construction there is no additional flow from the relative interior of V' (Lemma 4). We now handle flow into the cut-off pyramid coming from the boundary of V' by considering all possible cases. The polytope C is not driven into V'. We therefore do not add faces of V' to $\mathcal{V}$ if there intersection with C'° lies in V. If the driver d of V' lies on the boundary of V' then it has to be a critical point and is therefore not driven into V'. Any further point that is in C' but outside C'° is driven past it by the common driver d (Lemma 7). Therefore, any flow coming from the boundary of V' must come from points in C'° which are taken care of in line 6.

The recursion stops when there is no more inflow through higher dimensional Voronoi faces or through the boundary of a Voronoi face to consider.

Theorem 11. *Let c be a critical point of the distance function h and let V be the lowest dimensional Voronoi face containing c. Then* INFLOW$(\{c\}, V)$ *computes the stable manifold of c.*

Proof. First we show that the algorithm terminates. For this we need to prove that the depth of recursion can be bounded. If the recursion depth is at least m we get a sequence $(C_1, V_1), (C_2, V_2), \ldots, (C_{m-1}, V_{m-1}), (C_m, V_m) = (c, V)$ of pairs of polytopes and Voronoi faces, and a point $x \in C_1 \setminus C_2$ which flows through all the polytopes starting at C_1. By Theorem 9, x flows at most once through any Voronoi face. Therefore m is bounded by the complexity of the Voronoi diagram and the algorithm terminates.

Next we need to prove that the computed face S' is indeed the stable manifold S of c. From the description of the algorithm above it is clear that $S' \subseteq S$. If we assume $S \nsubseteq S'$ then there would be a point x which flows into c but is outside of S'. Since c is in S' the point x eventually must flow into S'. Assume the polytope C' is the polytope of S' into which x flows first. We may assume $C' \neq \{c\}$ and therefore C' has the form $C' = conv(C, d) \cap V$ with C a convex polytope, V a Voronoi face with $C^\circ \subset V^\circ$, and d the driver of V°.

Then x cannot flow into C' through the relative interior of V because it would be driven away by d. But x can also not come from a lower-dimensional Voronoi face because then it would either come through C which is part of S' or would be driven into V by d. But then the algorithm would have added the corresponding polytope to $\mathcal{I}$ in line 8 at the same time it added C'. The algorithm checks for flow from higher-dimensional Voronoi faces in the main loop, so x can also not flow into C' by a higher-dimensional face. Therefore x must already have been in S' and therefore $S \subset S'$. In total we have $S = S'$, i.e., the algorithm computes the stable manifold of c. □

5.3. Properties of the stable manifolds

The algorithm gives insight into the structure of the stable manifolds of critical points and the relationship between neighboring stable manifolds. Most importantly, the algorithm directly gives a polytopal decomposition of the closures of stable manifolds and therefore of the flow complex.

In the following we discuss the relationship between neighboring stable manifolds. Let S_1 and S_2 be the stable manifolds of the critical points c_1 and c_2, respectively. Let C_1 and C_2 be maximal polytopal faces of the closures of S_1 and S_2, respectively, and let $C_1 < C_2$, thus C_1 lies on the boundary of S_2. We denote this situation by $S_1 < S_2$.

We prove that in this case the critical point c_1 lies on the boundary of S_2 and c_1 has a smaller distance function value than c_2.

Lemma 12. *Let S_1 and S_2 be the stable manifolds of critical points c_1 and c_2, respectively. If $S_1 < S_2$, then c_1 lies on the boundary of S_2 and $h(c_1) < h(c_2)$.*

Proof. Suppose c_1 does not lie on the boundary of S_2. Then the orbit of any point in S_1 must eventually leave the boundary of S_2. Assume an orbit leaves the boundary at a point y. Then y is on the boundary of a polytopal face computed by the algorithm. Let C' be the first polytopal face of $\overline{S}_2$ computed by the algorithm with y on its boundary. We have $C' \neq \{c_2\}$. Thus C' is of the form $C' = conv(C, d) \cap V'$ with C a previously computed polytopal face of $\overline{S}_2$, V' the Voronoi face with $C'^\circ \subset V'^\circ$, and d the driver of V'°. The situation is illustrated in Fig. 9, where Fig. 9(a) shows the case where $d \notin V'$ and Fig. 9(b) the case where $d \in V'$.

We consider the different cases for the position of y on the boundary of C'. The case $y \in C$, e.g., y_1 in Fig. 9(a), is not possible by the assumption that C' was the first polytope found by the algorithm with y on its boundary. If y is in V'° (as y_3 in the example of Fig. 9(a) or d in the example of Fig. 9(b)) then y has d as a driver and the orbit of y does not leave C' at y. It remains the case that y is on the boundary of V' and the line segment $L_{d,y}$ does not intersect the interior of V' (as y_2 in Fig. 9(a)). Then by Lemma 7 the driver of y is d, thus y cannot flow away from C'.

Therefore, the orbit of a point in S_1 on the boundary of S_2 cannot leave the boundary of S_2, and the critical point c_1 of S_1 must lie on the boundary of S_2.

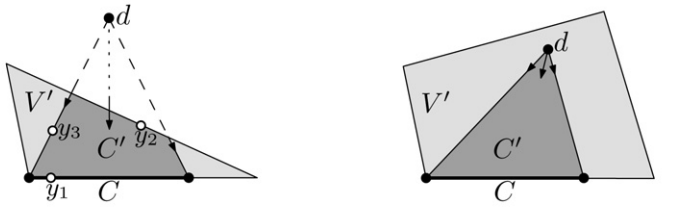

(a) $C' = conv(C, d) \cap V'$ with $d \notin V'$ (b) $C' = conv(C, d)$ and $d \in V'$

Fig. 9. Illustration of the proof of Lemma 12: a polytopal face C' of a stable manifold.

If we reconsider the case distinction for the position of a point y on the boundary of S_2 (Fig. 9), we see that $y \in \partial C' \setminus C$ can only be a critical point if it is actually the driver d of C'°. Thus the critical point c_1 is the driver d of a point $x \in S_2$ with $x \neq d$. By Lemmas 5 and 6 we have

$$h(c_1) \leqslant \pi_{c_1}(c_1) < \pi_{c_1}(x) = h(x).$$

The point x flows into c_2 and h increases in the direction of the flow, thus $h(x) \leqslant h(c_2)$ which proves the lemma. □

6. Topology of flow shapes

In the following we consider a filtration of the flow complex and its topology.

6.1. Families of parametrized shapes

Flow shapes. We have a natural filtration of the flow complex, i.e., a family of nested subcomplexes. By $F_\alpha(P)$ we denote the sub-complex of the flow complex that contains all stable manifolds of critical points at which the distance function h takes a value no more than $\alpha \geqslant 0$. The underlying space $|F_\alpha(P)|$ is called *flow shape*.

As discussed in Sections 1 and 2.3 further families of shapes and complexes are: The union of balls $|B_\alpha(P)|$, the Čech complex, and the α-shape complex. These families are parametrized by the distance level α and for a given distance level they are homotopy equivalent. In this section we prove that the flow shape $|F_\alpha(P)|$ is also homotopy equivalent to the union of balls. Before we proceed to the proof, we consider an example for these families.

Example. Fig. 10 shows the union of balls, the Čech complex, the α-shape complex, and the flow shape on α set P of unweighted points in two dimensions. Three different values for α are shown in the three columns of the figure.

In the first row the union of balls is shown together with their Voronoi diagram. In the left figure α is small and the balls are still isolated. In the middle figure α is larger and some of the balls already overlap. In the right figure α is very large, such that all balls overlap.

The second row shows the Čech complex. It is an abstract simplicial complex, so the placement of the points does not indicate a position in the plane but are chosen as for the union of balls to identify the vertices. Since in the left row the balls are isolated, the complex consists only of the vertices. In the middle figure it consists of vertices, edges, triangles, and a tetrahedron. The tetrahedron is in the complex since the four corresponding balls have a common intersection. In the right figure, the complex is not depicted: all subsets of points form a simplex since their balls have a common intersection. Thus the complex is the power set $\mathcal{P}(P)$, i.e., a 6-dimensional simplex.

In the next row the α-shape complex is depicted. It contains only simplices for intersecting balls that also have a Voronoi face in common. For the isolated balls in the left row, the α-shape complex is again the set of points. In the middle figure it contains of the 3-simplex of the Čech complex only the two Delaunay triangles. In the right figure the α-shape complex equals the Delaunay tessellation of the points.

The bottom row shows the flow complex filtration. Again it starts with the set of points. In the middle figure several edges (stable manifolds of saddle points) and one two-dimensional face (the stable manifold of a maximum). In contrast to the α-shape complex this face is not decomposed into two triangles, since it contains only one critical point. Also the further triangle which is present in the α-shape complex is not contained since it does not correspond to a critical point. In the right figure, one additional face is present, the stable manifold of the second local maximum.

6.2. Homotopy equivalence of union of balls and flow shapes

We prove the homotopy equivalence of the union of balls and flow shape for a distance level α in several steps. First we consider the levels α between two critical levels. Here the homotopy type of both complexes does not change. Thus, we only need to consider critical levels. We separately consider how the union of balls and how the flow shape change at critical levels, and then combine this information to prove by induction over the critical values that the two complexes have the same homotopy type.

Between critical levels. By definition the flow shapes do not change between the critical values of the distance function. From the critical point theory of distance functions we get that an isotopy lemma as in Morse theory still holds (Proposition 1.8 in [15]), i.e., the homotopy of the union of balls does not change between critical values.

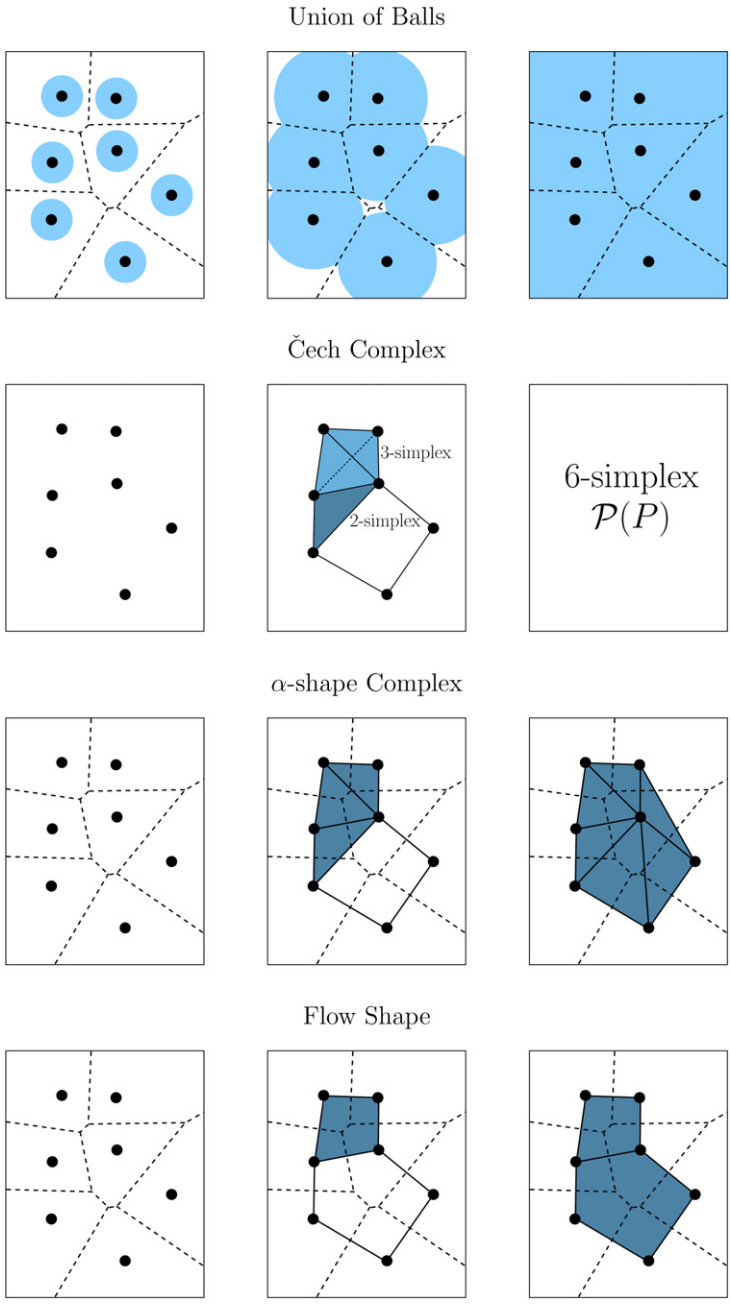

Fig. 10. Example of parametrized shapes and complexes.

Lemma 13 *(Isotopy Lemma). If the interval* $[\alpha, \alpha') \subset [0, \infty)$ *does not contain any critical value of* h*, i.e., there is no critical point* $x \in \mathbb{R}^k$ *of* h *with* $h(x) \in [\alpha, \alpha')$*, then* $|B_\alpha(P)|$ *is homeomorphic to* $|B_{\alpha'}/(P)|$*, and* $|B_\alpha(P)|$ *is a deformation retract of* $|B_{\alpha'}(P)|$*.*

Union of balls at a critical level. The following lemma describes how the homotopy of the union of balls changes at critical values. The union of balls with parameter $\alpha + \varepsilon$ above a critical level α can be continuously deformed to the union of balls with parameter $\alpha - \varepsilon$ below the critical level with a small part of a Delaunay simplex glued in at each position of critical points at this level. We will use this later to glue in the same part into a flow shape.

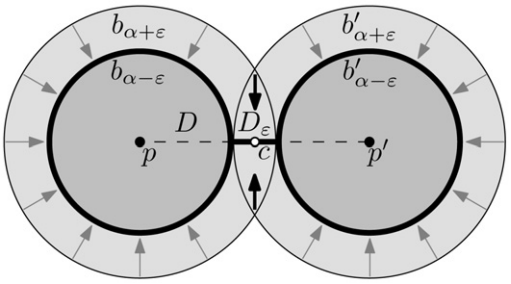

Fig. 11. The set $b_{\alpha-\varepsilon} \cup b'_{\alpha-\varepsilon} \cup D_\varepsilon$ is a deformation retract of $b_{\alpha+\varepsilon} \cup b'_{\alpha+\varepsilon}$.

The configuration at a critical point is illustrated in Fig. 11. It shows a critical point c defined by the two points p and p'. The distance level of c is α, i.e., both the distance from p to c and from p' to c is $\sqrt{\alpha}$. Therefore the unions of balls $|B_{\alpha-\varepsilon}| = b_{\alpha-\varepsilon} \cup b'_{\alpha-\varepsilon}$ and $|B_{\alpha+\varepsilon}| = b_{\alpha+\varepsilon} \cup b'_{\alpha+\varepsilon}$ are not homotopy equivalent. The points p and p' define a Delaunay face D. The part of D that we add to the smaller union of balls is $D_\varepsilon := D \setminus B_{\alpha-\varepsilon}$.

Now $|B_{\alpha+\varepsilon}|$ can be shrunk to $|B_{\alpha-\varepsilon}| \cup D_\varepsilon$ in the following way. In the proximity of a critical point an orthogonal shrinking is chosen as indicated by the two black arrows in the figure. Outside of the proximity of any critical point a radial shrinking is chosen as indicated by the gray arrows. The different types of shrinking can be combined by a partition of unity.

Instead of constructing the shrinking explicitly we will again apply the critical point theory for distance functions. If the direction of the arrows in Fig. 11 are reverted, they indicate a set of generalized gradients for $|B_{\alpha-\varepsilon}| \cup D_\varepsilon$ (which are not necessarily gradients). The following lemma generalizes an observation by Siersma [23] for the union of disks in two dimensions (cf. also Lemma 1.13 in [15]).

Lemma 14. *Let α be a critical value of the distance function and $c_1, \ldots, c_m$ with $m \geqslant 1$ the critical points at value α. Let V_i be the lowest dimensional Voronoi face containing c_i and D_i the dual Delaunay face for $1 \leqslant i \leqslant m$.*

There is an $\varepsilon > 0$ such that $D_{i,\varepsilon} := D_i \setminus |B_{\alpha-\varepsilon}|$ is a topological ball (of the same dimension as D_i) containing c_i for $1 \leqslant i \leqslant m$, and $|B_{\alpha-\varepsilon}| \cup D_{1-\varepsilon} \cup \cdots \cup D_{m,\varepsilon}$ is a deformation retract of $|B_{\alpha+\varepsilon}|$.

Proof. We first restrict us to the case of one critical point c, with V the lowest dimensional Voronoi face containing c, D the dual Delaunay face D, and $D_\varepsilon := D \setminus |B_{\alpha-\varepsilon}|$ (as in Fig. 11). Then we generalize the argument to a set of critical points.

Since c is a critical point and therefore its own driver, c is contained in D_ε. Let U be the union of the Voronoi cells of the vertices of D. Since $c \in V^\circ$, a neighborhood of c is contained in U°. Let $\varepsilon > 0$ be chosen such that the interval $[\alpha - \varepsilon, \alpha + \varepsilon]$ contains no critical value except α and that a $\sqrt{2\varepsilon}$-neighborhood of $\overline{D}_\varepsilon$ is contained in U°.

Instead of applying the critical point theory of distance functions to P we apply it to the compact set K with

$$K := P \cup \overline{D}_\varepsilon.$$

The weights of all points in $\overline{D}_\varepsilon$ is set to $\varepsilon - \alpha$.

We prove that the levels α' with

$$\alpha - \varepsilon < \alpha' \leqslant \alpha + \varepsilon$$

are regular for the distance function h_K of K.

At the distance level $\alpha + \varepsilon$ the influence of $\overline{D}_\varepsilon$ is limited to an $\sqrt{2\varepsilon}$-neighborhood of $\overline{D}_\varepsilon$ and therefore by construction limited to U°. Points outside of this neighborhood in $|B_{\alpha+\varepsilon}| \setminus |B_{\alpha-\varepsilon}|$ are regular for h_K.

For a point $x \in U^\circ \setminus \mathit{aff}(D)$ let $N_K(x)$ denote the set of closest points in K to x. Since $N_K(x)$ is contained in D, the vector pointing orthogonally away from $\mathit{aff}(D)$ forms an angle less than $\pi/2$ with the vectors from the points in $N_K(x)$ to c. Thus, this vector is a generalized gradient at x and x is a regular point of h_K (see Section 3.1).

By the critical point theory for distance functions [15] this yields that the level sets $h^{-1}(\alpha')$ are homeomorphic, and $|B_{\alpha+\varepsilon}|$ can be deformation retracted to K. For the above argument, only the generalized gradients in a small neighborhood of c had to be considered. If we define $K' := P \cup \overline{D_{1,\varepsilon}} \cup \cdots \cup \overline{D_{m,\varepsilon}}$ and consider h'_K the argumentation

directly generalizes to a set of critical points by choosing $\varepsilon > 0$ in such a way that the $\sqrt{2\varepsilon}$-neighborhoods of the $\overline{D_{i,\varepsilon}}$ $(i = 1, \ldots, m)$ do not overlap. □

Flow shape at a critical level. For the union of balls we can describe the change of topology at a critical level by gluing in neighborhoods of the critical points. We have an analogous result for flow shapes: By taking out small neighborhoods out of the shape at the critical level, we can retract it to the shape of the previous critical level.

Lemma 15. *Let α be a critical value of the distance function and $c_1, \ldots, c_m$ with $m \geqslant 1$ the critical points at value α. Let V_i be the lowest dimensional Voronoi face containing c_i and D_i the dual Delaunay face for $1 \leqslant i \leqslant m$.*

There is an $\varepsilon > 0$ such that $|F_{\alpha-\varepsilon}|$ is a deformation retract of $|F_\alpha| \setminus (D_{1,\varepsilon} \cup \cdots \cup D_{m,\varepsilon})$ where $D_{i,\varepsilon} := D_i \setminus |B_{\alpha-\varepsilon}|$ for $1 \leqslant i \leqslant m$.

Proof. We present a deformation retract using the structure of stable manifolds inherently described by the algorithm INFLOW. We retract maximal polytopal faces of a stable manifold S one at a time such that $\overline{S} \setminus D_\varepsilon$ is retracted to the faces it shares with the closures of stable manifolds S' with $S' < S$. By Lemma 12 these stable manifolds are present in F_α. For the deformation retraction it is necessary that co-faces of the polytopal faces of S that we want to retract are not yet present in the restricted flow complex. This is guaranteed by Lemma 12. In particular, the stable manifolds of the same critical level do not influence each other. We can therefore restrict us to the case of one critical point at the critical level α. In the case of several critical points we can retract them one at a time.

Let $\varepsilon > 0$ be chosen such that the interval $[\alpha - \varepsilon, \alpha + \varepsilon]$ contains no critical value except α. Let c be the critical point at level α, S its stable manifold, V the lowest dimensional Voronoi face containing c, D the dual Delaunay face, and $D_\varepsilon := D \setminus |B_{\alpha-\varepsilon}|$.

The steps of the deformation retract are illustrated in Fig. 12 by the example of the weighted two-dimensional point set previously used. In the example we want to retract the stable manifold corresponding to the two-dimensional part of the flow complex. In Fig. 12(a)–(d) always the parts that have been already retracted are labeled while the remaining part is shown shaded in gray.

Fig. 12 (a) shows the stable manifold with D_ε removed.

The algorithm INFLOW successively processes a sequence of Voronoi faces (its second argument). For the proof we rearrange the order of processing these Voronoi faces in a breadth first manner: we collect all flow from higher dimensional Voronoi faces before we collect flow from the boundary of a Voronoi face. For the implementation this means instead of using a stack as it is implicitly done with the recursive calls we use a queue.

This gives us a hierarchy as follows: we start with a point (the critical point) and a Voronoi face V that contains the point. Then we process all Voronoi faces that contain V together with some higher dimensional polytope. Whenever we process new flow coming from the boundaries of previously processed Voronoi cells a new step in the hierarchy starts. Assume that we have N steps in the hierarchy and let S_j, $j = 1, \ldots, N$, be the interior of the part of the stable manifold S of c that has been constructed after finishing step j of the hierarchy. In the example of Fig. 12 we have three parts of the stable manifold S in the hierarchy: S_1 is the part reached without crossing the boundary of a Voronoi cell. Then S_2 additionally includes the lower left triangle of the remaining part and $S_3 = S$ the right triangle.

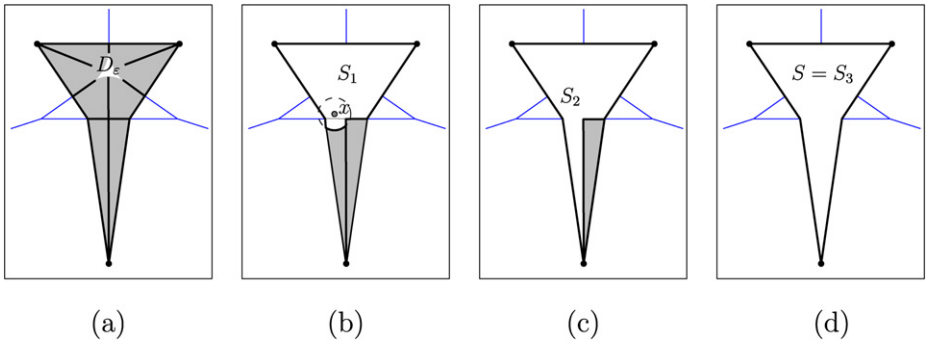

Fig. 12. Steps in the deformation retract in the proof of Lemma 15.

We show by induction over N that $\overline{S} \setminus D_\varepsilon$ deformation retracts to $\overline{S} \setminus S_N = \overline{S} \setminus S = \partial S$. Note that deformation retractions are transitive in the sense that if X_1 is a deformation retraction of X_2, and X_2 is a deformation retraction of X_3 then X_1 is a deformation retraction of X_3.

We first show that $\overline{S} \setminus D_\varepsilon \simeq \overline{S} \setminus S_1$ holds by a deformation retract. For this consider the boundary ∂S_1 of S_1. It has the structure of a polyhedral complex and is visible from the critical point. With D_ε removed we can therefore retract (radially from c) to the boundary of S_1.

For the induction step we construct a deformation retract from $\overline{S} \setminus S_j$ to $\overline{S} \setminus S_{j+1}$ for $1 \leqslant j < N$. For this we consider a cell C of $\partial S_j \cap S_{j+1}$ together with the corresponding Voronoi face V. We proceed by showing that the area C' of flow onto C from higher-dimensional Voronoi faces can be retraced starting at C. We cannot directly follow the direction of flow since the boundary should stay fixed. Instead we use the following retraction: we choose a point x that is outside of C' and that sees all interior points of C' through the interior of C (i.e., the line through x and any point in the interior of C' intersects C). Such a point exists (close to C) since C' is a convex polytope with C as a facet. Now C' can be retracted starting at C radially away from x until a boundary of C' (other than C) is hit. This process is shown in Fig. 12(b) for the case $j = 1$. In the figure, S_1 has been already removed and C has been radially pushed away from x. The original position of C is shown as dotted line segment.

Lower dimensional parts of S_j might remain which we can easily retract. In the example of the figure this is not necessary for S_2 but in the next step, i.e., when the right triangle is retracted, the middle segment remains which then is retracted. From this we get a deformation retract from $\overline{S} \setminus S_j$ to $\overline{S} \setminus S_{j+1}$ for $1 \leqslant j < N$, and by induction a deformation retraction from $\overline{S} \setminus D_\varepsilon$ to $\overline{S} \setminus S_N = \partial S$. Fig. 12(d) shows the situation where all of $S = S_3$ has been retracted to its boundary. □

Homotopy equivalence. We are now prepared to prove the main theorem of this section.

Theorem 16. *Let P be a finite set of weighted points in $\mathbb{R}^k$. For every $\alpha \geqslant 0$ the flow shape $|F_\alpha(P)|$ is homotopy equivalent to the union of balls $|B_\alpha(P)|$.*

Proof. The homotopy type of both $|B_\alpha(P)|$ and $|F_\alpha(P)|$ changes only at critical values of the distance function h, and $|F_\alpha(P)|$ only changes at these levels at all. For levels α, α' between two critical levels $|B_\alpha(P)|$ is a deformation retraction of $|B'_\alpha(P)|$ by the isotopy lemma (Lemma 13).

Thus, it suffices to check that $|F_\alpha(P)|$ stays homotopy equivalent to $|B_\alpha(P)|$ if α pass a critical level.

We prove by induction that for all critical values α, $|F_\alpha(P)|$ is a deformation retraction of $|B_{\alpha+\varepsilon}(P)|$ for a suitable $\varepsilon > 0$.

Without loss of generality we assume that all points have non-positive weights and the largest weight is 0. This can be achieved by subtracting the largest weight from all others. Thus, h is positive and 0 is the smallest critical value.

Let $0 = \alpha_0 < \alpha_1 < \cdots < \alpha_n$ be the critical values of h. Note that there can be only finitely many critical points of h by Lemma 4. Assume that $|F_\alpha(P)|$ is a deformation retraction of $|B_\alpha(P)|$ for all $\alpha \leqslant \alpha_{i-1} + \varepsilon$, where $\varepsilon > 0$ is chosen such that it satisfies the following:

(i) The ε-neighborhood of any critical value α_j $(0 \leqslant j \leqslant n)$ does not contain any other critical value.
(ii) $0 < \varepsilon < \min\{\varepsilon_c \mid c \text{ a critical point}\}$, where $\varepsilon_c > 0$ is chosen such that $D_{i,\varepsilon_c} \subset S$, where D_{i,ε_c} is defined as before (see Lemma 14). The existence of such an ε_c follows from the recursive construction of the stable manifold S of c in the algorithm INFLOW.

For $\alpha_0 = 0$ we have $|B_{\alpha_0}(P)| = P_0 = |F_{\alpha_0}(P)|$, where P_0 is the set of points of weight 0. By retracting balls to points, we get that $|F_{\alpha_0}(P)|$ is a deformation retraction of $B_{\alpha_0+\varepsilon}$.

In the induction step, we need to prove that $|F_{\alpha_i}(P)|$ is a deformation retraction of $|B_{\alpha_i+\varepsilon}(P)|$. By the induction hypothesis we have that $F_{\alpha_{i-1}}(P)|$ is a deformation retraction of $B_{\alpha_{i-1+\varepsilon}}(P)|$. By the isotopy lemma (Lemma 13) we have for all $\alpha_{i-1} + \varepsilon \leqslant \alpha' < \alpha_i$ that $|B_{\alpha_{i-1+\varepsilon}}(P)|$ is a deformation retraction of $|B_{\alpha'}(P)|$. Thus $|F_{\alpha'}(P)| = |F_{\alpha_{i-1}}(P)|$ is a deformation retraction of $|B_{\alpha'}(P)|$.

Let $c_1, \ldots, c_m$ be the critical points of h at α_i and $D_{1,\varepsilon}, \ldots, D_{m,\varepsilon}$ defined as before (see Lemma 14).

We construct the deformation retraction in two steps: In the first step we prove that

$$A := \big|F_{\alpha_i}(P)\big| \setminus (D_{1,\varepsilon} \cup \cdots \cup D_{m,\varepsilon})$$

is a deformation retraction of

$$X := \left|B_{\alpha_i-\varepsilon}(P)\right|.$$

In the second step we extend this deformation retraction of $|F_{\alpha_i}(P)|$ to $|B_{\alpha_i+\varepsilon}(P)|$.

For the first step we use Remark 2. We have $A \subset X$. By taking for a sufficiently small $\varepsilon' > 0$ an ε'-neighborhood of A in X we get a mapping cylinder neighborhood of A in X. The required properties directly follow from the critical point theory of distance functions applied to the distance function of A.

We need to prove that the inclusion $\iota : A \hookrightarrow X$ is a homotopy equivalence. Thus we need a map $g : X \to A$ such that

$$\iota \circ g \simeq id_X \quad \text{and} \quad g \circ \iota \simeq id_A.$$

Let $G : X \times [0,1] \to X$ be the deformation retraction of X to $|F_{\alpha_{i-1}}(P)|$ given by the induction hypothesis. Let $g : X \to A$ be defined by $g(x) = G(x,1)$. The map $\iota \circ g$ is simply $G(\cdot,1) : X \to X$ and therefore by induction hypothesis homotopic to id_X.

The map $g \circ \iota$ is the restriction of g to A and therefore maps A to $|F_{\alpha_{i-1}}(P)|$. By Lemma 15, $|F_{\alpha_{i-1}}(P)|$ is a deformation retract of A, thus the map $g \circ \iota$ is homotopic to id_A.

By Remark 2, A is a deformation retraction of X. The retract is constant on

$$\partial D_{1,\varepsilon} \cup \cdots \cup \partial D_{m,\varepsilon}$$

since this union is in A. We can extend the deformation retraction by the identity map on $(D_{1,\varepsilon} \cup \cdots \cup D_{m,\varepsilon})$ to a deformation retraction from

$$X' := |B_{\alpha_i-\varepsilon}(P)| \cup D_{1,\varepsilon} \cup \cdots \cup D_{m,\varepsilon} = X \cup D_{1,\varepsilon} \cup \cdots \cup D_{m,\varepsilon}$$

to

$$A' := \left|F_{\alpha_i}(P)\right| = A \cup D_{1,\varepsilon} \cup \cdots \cup D_{m,\varepsilon}.$$

By Lemma 14, X' is a deformation retraction of $|B_{\alpha_i+\varepsilon}|$. This concludes the induction. We have proved that between any two critical levels the homotopy type of the flow shape and the union of balls are the same. Since the homotopy type only changes at critical levels, it also has to be the same at the critical levels. We therefore have for all levels α of the distance function h that $|F_\alpha(P)| \simeq |B_\alpha(P)|$. □

7. Conclusion

We presented an algorithm for computing the flow complex in any dimension and a proof of the homotopy equivalence of the unions of balls and flow shapes based on this algorithm. This places flow shape in a class of topologically equivalent shape constructors. In their geometry these shape constructors can be quite different as is illustrated in Fig. 13 by a comparison to α-shapes. The pictures for Fig. 13 were produced with our implementations of efficient algorithms to compute the α-shape and the flow shape, respectively, in $\mathbb{R}^3$. Also this figure shows the union of balls at the corresponding levels. Notice that this union looks almost like a big ball at large levels. The level here is so large that we had to zoom out in order to fit the union of balls on the screen.

Acknowledgements

We like to thank Britta Denner-Broser for discussing the proof of Theorem 15 and Maike Buchin and Günter Rote for proof-reading. We also thank the anonymous reviewers for their comments that helped to improve the paper.

Appendix A. Table of notation

P	set of (weighted) input points in $\mathbb{R}^k$
p, q	points in P
w_p, w_q	weights/powers of p, q
x, y, z	points in $\mathbb{R}^k$

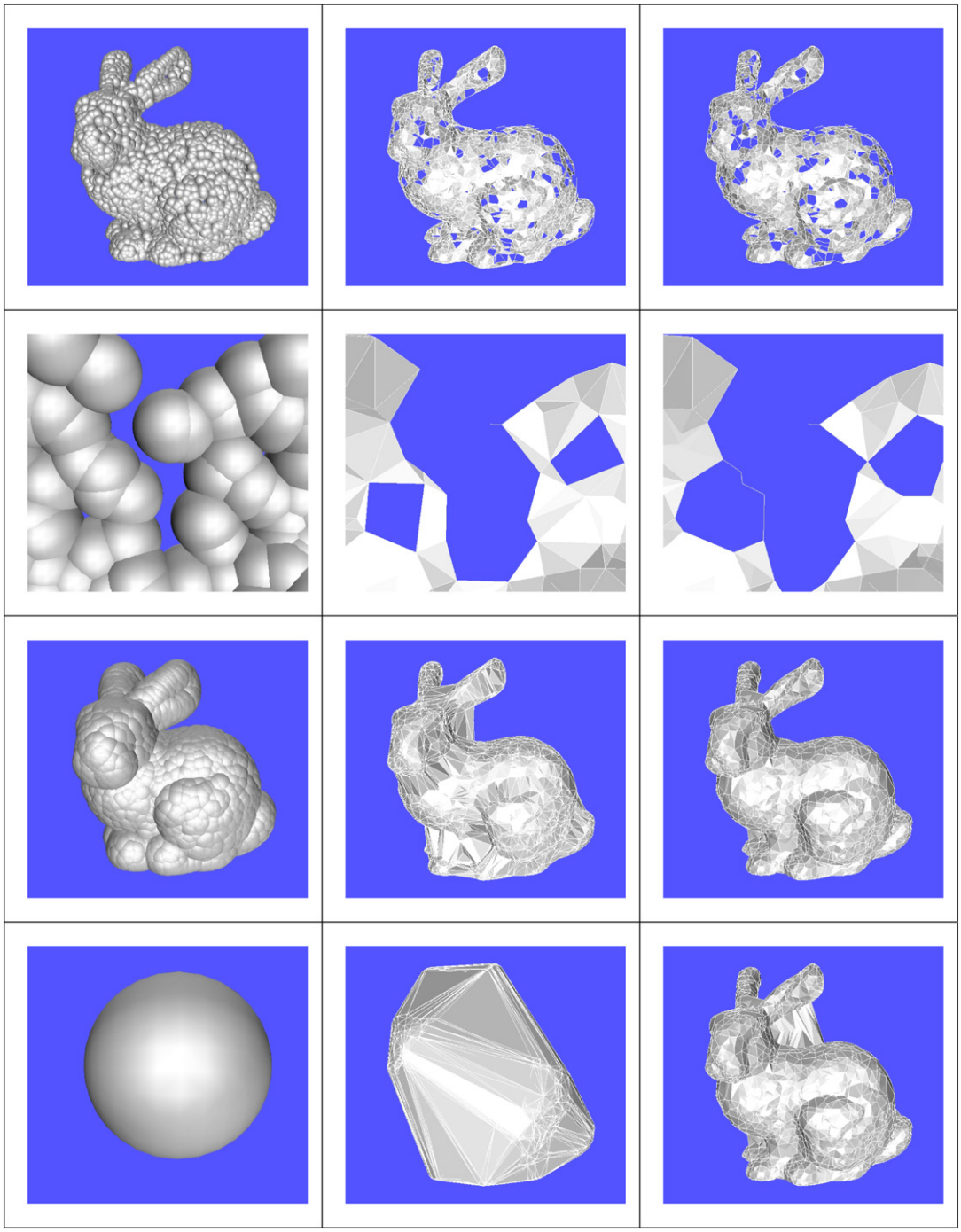

Fig. 13. The union of balls (left), the α-shape (middle) and the flow shape (right) for increasing values of α (top to bottom). The second row shows a zoom of the pictures in the first row. Note that the shapes in each row are homotopy equivalent.

C, C'	convex sets in $\mathbb{R}^k$
$\overline{X}$	closure of X
X°	relative interior of X
∂X	relative boundary of X
$conv(X)$	convex hull of X

$aff(X)$ affine hull of X
V, V', V_p Voronoi faces
D, D' Delaunay faces (dual to V, V')
$\mathcal{V}, \mathcal{V}'$ sets of Voronoi faces
$V \leqslant V'$ V is a face of V' (and V' a co-face of V)
$\pi_p(x)$ power distance
$h(x)$ distance function
$N(x)$ set of nearest neighbors
$v(x)$ unit vector field
$\phi(t, x)$ flow (at time t on the flow line of x)
$d, d', d(x)$ drivers (of x)
w_d power of the driver d
S, S_i stable manifolds
α distance value
$F_\alpha(P)$ sub-complex of the Flow complex
$B_\alpha(P)$ set of balls
$\check{C}_\alpha(P)$ Čech complex
$f \simeq g$ f and g are homotopic
$X \simeq Y$ X and Y are homotopy equivalent

References

[1] G.E. Bredon, Topology and Geometry, Graduate Texts in Mathematics, vol. 139, Springer, New York, Heidelberg, Berlin, 1993.
[2] K. Buchin, J. Giesen, Flow complex: General structure and algorithm, in: Proceedings of the 17th Canadian Conference on Computational Geometry (CCCG'05), 2005, pp. 270–273.
[3] G. Carlsson, V. de Silva, Topological approximation by small simplicial complexes, Manuscript, 2003.
[4] J. Cheeger, Critical points of distance functions and applications to geometry, in: P. de Bartolomeis, F. Tricerri (Eds.), Geometric Topology: Recent Developments, in: Lecture Notes in Mathematics, vol. 1504, Springer, 1991, pp. 1–38.
[5] T.K. Dey, J. Giesen, S. Goswami, Shape segmentation and matching with flow discretization, in: Proc. 8th Intern. Workshop on Algorithms and Data Structures, 2003, pp. 25–36.
[6] T.K. Dey, J. Giesen, M. John, Alpha-shapes and flow shapes are homotopy equivalent, in: Proc. 35th Symp. Theory of Computing, ACM, 2003, pp. 493–501.
[7] H. Edelsbrunner, The union of balls and its dual shape, Discrete Computational Geometry 13 (1995) 415–440.
[8] H. Edelsbrunner, Geometry and Topology for Mesh Generation, Cambridge Monographs on Applied and Computational Mathematics, Cambridge University Press, 2001.
[9] H. Edelsbrunner, Surface reconstruction by wrapping finite sets in space, in: B. Aronov, S. Basu, J. Pach, M. Sharir (Eds.), Discrete and Computational Geometry. The Goodman–Pollack Festschrift, in: Algorithms and Combinatorics, vol. 25, Springer, 2003, pp. 379–404.
[10] H. Edelsbrunner, M. Facello, J. Liang, On the definition and the construction of pockets in macromolecules, Discrete Appl. Math. 88 (1–3) (1998) 83–102.
[11] H. Edelsbrunner, D. Kirkpatrick, R. Seidel, On the shape of a set of points in the plane, IEEE Trans. Inform. Theory IT-29 (4) (1983) 551–559.
[12] J. Giesen, M. John, Computing the weighted flow complex, in: Proc. 8th International Fall Workshop Vision, Modeling, and Visualization, 2003, pp. 235–243.
[13] J. Giesen and M. John, The flow complex: A data structure for geometric modeling, in: Proc. 14th ACM-SIAM Sympos. Discr. Algorithms, 2003, pp. 285–294.
[14] M. Goresky, R. MacPherson, Stratified Morse Theory, Ergebnisse der Mathematik und ihrer Grenzgebiete, 3. Folge, vol. 14, Springer, 1988.
[15] K. Grove, Critical point theory for distance functions, in: Differential Geometry: Riemannian Geometry, in: Proc. Sympos. Pure Math., vol. 54, Amer. Math. Soc., 1993, pp. 357–385.
[16] K. Grove, K. Shiohama, A generalized sphere theorem, Ann. of Math. 106 (1977) 201–211.
[17] A. Hatcher, Algebraic Topology, Cambridge University Press, 2002.
[18] J. Leray, Sur la forme des espaces topologiques et sur les points fixes des représentations, J. de Math. 24 (1945) 95–167.
[19] J. Matoušek, Lectures on Discrete Geometry, Springer, 2002.
[20] J.W. Milnor, Morse Theory, Annals of Mathematics Studies, vol. 51, Princeton University Press, Princeton, NJ, 1963.
[21] A. Okabe, B. Boots, K. Sugihara, S.N. Chiu, Spatial Tesselations: Concepts and Applications of Voronoi Diagrams, second ed., Wiley, 2000.
[22] P. Petersen, Riemannian Geometry, Graduate Texts in Mathematics, vol. 171, Springer, 1998.
[23] D. Siersma, Voronoi diagrams and Morse theory of the distance function, in: Geometry in Present Day Science, World Scientific, 1999, pp. 187–208.
[24] E.H. Spanier, Algebraic Topology, McGraw-Hill Series in Higher Mathematics, McGraw-Hill, New York, 1966.

[25] G.M. Ziegler, Lectures on Polytopes, Graduate Texts in Mathematics, Springer, 2001.
[26] A.J. Zomorodian, Topology for Computing, Cambridge Monographs on Applied and Computational Mathematics, Cambridge University Press, 2005.